Water Environment Research

RESEARCH ARTICLE OPEN ACCESS

Adsorption Performance of Zn(II)-Based Coordination Polymer (ZnMOF) Reinforced Magnetic Activated Biochar (CmBC-Fe_3O_4@ZnMOF) Hybrid Composites

Muradiye Şahin[1,2] | Yasin Arslan[2] | Muhammet Atasoy[3] | Mika Sillanpää[4]

[1]Department of Chemistry, Kırşehir Ahi Evran University, Kırşehir, Turkey | [2]Faculty of Arts and Science, Department of Nanoscience and Nanotechnology, Burdur Mehmet Akif Ersoy University, Burdur, Turkey | [3]Chemistry and Chemical Treatment Technologies Department, Chemistry Technology Program, Muğla Sıtkı Koçman University, Muğla Vocational School, Muğla, Turkey | [4]Department of Biological and Chemical Engineering, Aarhus University, Aarhus, Denmark

Correspondence: Muradiye Şahin (muradiye.sahin@ahievran.edu.tr)

Received: 15 February 2025 | **Revised:** 15 May 2025 | **Accepted:** 3 June 2025

Funding: This study was supported by the TUBITAK (The Scientific and Technological Research Council of Turkey) 2218 Project (122C199).

Keywords: adsorption | coordination polymer | hybrid material | in situ method | modification

ABSTRACT

Evaluation of organic wastes originating from livestock as biochar is of great importance in terms of both economic and environmentally friendly sustainable material production. In this study, cow manure (C_m), an animal waste, was used for biochar (BC) production. The obtained biochar was activated with Fe_3O_4 and given magnetic properties (CmBC-Fe_3O_4), then modified with a Zn(II)-based coordination polymer (ZnMOF) to synthesize a hybrid material, CmBC-Fe_3O_4@ZnMOF. The synthesis of this innovative hybrid material was carried out in two stages: In the first stage, CmBC-Fe_3O_4 was obtained by in situ synthesis method. In the second stage, it was modified with ZnMOF synthesized by solvothermal method to obtain the innovative adsorbent of CmBC-Fe_3O_4@ZnMOF hybrid material. The synthesized CmBC-Fe_3O_4, ZnMOF, and CmBC-Fe_3O_4@ZnMOF were characterized by scanning electron microscopy equipped with energy dispersive X-ray spectrometry (SEM–EDX), X-ray diffraction analysis (XRD), Fourier transform infrared spectroscopy (FTIR), TG/DTA, and BET analyses. Based on kinetic feasibility, CmBC-Fe_3O_4@ZnMOF has the highest removal efficiency. The removal efficiencies of Pb(II), Cd(II), Cu(II), and Mn(II) in the synthetic water sample were found to be 81.39%, 69.52%, 58.47%, and 32.53%, respectively. On the other hand, the corresponding removal efficiencies in the milk sample were found to be 64.63%, 43.02%, 30.62%, and 19.27%, respectively. Isotherm (Dubinin–Radushkevich, Freundlich, and Langmuir) and kinetic (Elovich, Ho-McKay, and Lagergren) models were used and mostly fit with Ho-McKay second-order rate equation and the Freundlich isotherm model. In addition, the reusability studies were carried out in three cycles, and it was observed that it can be used after three cycles without losing its efficiency. It was concluded that the CmBC-Fe_3O_4@ZnMOF hybrid material is an effective adsorbent with the potential to remove heavy metals from both water and milk solutions and its selectivity for Pb(II) and Cd(II) is higher than that for Cu(II), and Mn(II).

Summary

- Hybrid material (CmBC-Fe_3O_4@ZnMOF) structures combining unit cells with different adsorption capacities.
- Zn(II)-based coordination polymer (ZnMOF) and activated magnetic biochar (CmBC-Fe_3O_4) were used to evaluate their performance on heavy metal removal from milk and synthetic water samples.
- CmBC-Fe_3O_4 was synthesized by a one-step in situ synthesis method and ZnMOF by solvothermal method.

- CmBC-Fe_3O_4@ZnMOF showed excellent and selective adsorption capacity especially for Pb(II) and Cd(II).
- The removal efficiencies for Pb(II), Cd(II), Cu(II), and Mn(II) in synthetic water sample were found to be 81.39%, 69.52%, 58.47%, and 32.53%, respectively.
- The removal efficiencies for Pb(II), Cd(II), Cu(II), and Mn(II) in milk sample were found to be 64.63%, 43.02%, 30.62%, and 19.27%, respectively.

1 | Introduction

The presence of heavy metals, such as lead (Pb), cadmium (Cd), copper (Cu), and manganese (Mn) in both water and milk samples, is a serious environmental and public health problem (Aziam et al. 2024; Şahin et al. 2023; Şahin and Arslan 2023a; Feizi et al. 2022). The reasons for the presence of these metals in water include industrial wastes, mining activities, chemicals used in agriculture, and domestic wastes (Şahin et al. 2023; Şahin and Arslan 2023a; Zamora-Ledezma et al. 2021). These heavy metals can dissolve in water, milk, and contaminate drinking water supplies, leading to toxic effects on human health (Ogamba et al. 2021; Ren et al. 2022). In principle, Pb and Cd can cause both neurological damage and kidney problems (Şahin et al. 2023; Şahin and Arslan 2023a; Zhao et al. 2019a), while Cu and Mn can have adverse effects on the both liver and nervous system when overexposed (Zhao et al. 2019b; Fato et al. 2019; Adenuga et al. 2019; Semerjian 2018). For these reasons, the detection and removal of heavy metals is an important issue. The literature studies show that various techniques, such as chemical precipitation (Tian et al. 2020), ion exchange (C. Yang, Ju, et al. 2020), membrane filtration (Liu et al. 2020), electrolysis (Chen et al. 2020), and adsorption (Xu et al. 2018; Şahin et al. 2024; Şahin and Arslan 2023b) have been used in recent years to remove heavy metals from the environment. Among these techniques, adsorption is a suitable alternative to traditional water treatment methods due to its advantages, such as less waste generation, low-cost, simplicity of processes, selective removal, reusability of adsorbent, and ability to remove micropollutants at low concentrations (Zhang et al. 2020).

Various materials, such as nanoparticles (El-Dib et al. 2020), carbon nanotubes (Hayati et al. 2018), activated carbon (Shahrashoub and Bakhtiari 2021), biochar (Peng et al. 2017), graphene oxide (Lebron et al. 2020), clay (Khalfa et al. 2021), and biosorbent (Adenuga et al. 2019) are commonly utilized as adsorbents for the removal of heavy metals from aqueous solutions through adsorption. Among these, biochar (BC) has garnered significant research interest in recent years due to its numerous advantages, including ease of preparation, cost-effectiveness, high reusability, and environmental sustainability (Yaashikaa et al. 2020). BC is a carbon-rich material usually produced by the thermal decomposition of biomass under oxygen-limited conditions. The surface chemistry and textural properties of BC are influenced by factors, such as biomass type, heat treatment, and production method (Silos-Llamas et al. 2020). Due to its abundant surface functional groups (e.g., amide, carboxyl, carbonyl, hydroxyl, and alkyne) and well-developed pore structure, BC is widely used as an adsorbent for the adsorption of many pollutants (Shan et al. 2020). In addition to food, agricultural, forestry, and municipal solid waste, animal manure is also used as biomass for BC production (Varjani et al. 2019; Kumar et al. 2013). The cow manure contains a large amount of undigested lignin and cellulose, which is a natural carbon source. BC obtained by cow manure can be used as an effective adsorbent to remove dyes, heavy metals, toxic inorganic anions, and other environmental pollutants (Varjani et al. 2019; Kharel et al. 2019; Wan et al. 2018; Chen, Qin, Sun, et al. 2018). As a major source of solid waste from the livestock industry (Chen, Qin, Sun, et al. 2018), cow manure carries a high risk of pathogen transmission and infection, and its disposal is considered as a major challenge for the livestock and agricultural industries (Qin et al. 2016). The livestock and agriculture sector involves not only organic waste production but also multifaceted health and environmental risks, such as antibiotic resistance, contamination of water resources, and greenhouse gas emissions (Jose 2009; Jungbluth et al. 2001). Agricultural and livestock activities also cause negative impacts on the ecosystem, such as biodiversity loss, water scarcity, and soil degradation (Rockström et al. 2009). In addition, improper processing of animal manure increases environmental pollution along with the spread of zoonotic diseases, posing a serious threat to sustainable agriculture (Li et al. 2021). In this context, the development of sustainable waste management strategies has become a priority goal both environmentally and economically. In this study, the use of cow manure produced in the livestock farm established at Burdur Mehmet Akif Ersoy University will contribute to the utilization of biomass wastes left to decompose, converting them into high value-added products and eliminating the wastes that cause environmental pollution. In many studies, biochars have been modified (Li et al. 2018) or activated (Liu et al. 2020) with various chemical agents, such as Ca $(OH)_2$, KOH, H_3PO_4, H_2SO_4, and $ZnCl_2$ to increase their surface areas and adsorption performances. In this study, iron salts ($FeCl_3{\cdot}6H_2O$ and $FeSO_4{\cdot}7H_2O$) were added and simultaneous pyrolysis was carried out during biochar production in order to both increase the surface area and gain magnetic properties. Due to their advantages of tunable chemical properties, ordered crystal structure, large specific surface area, and high porosity (Chen et al. 2022; Mondol and Jhung 2021; Wen et al. 2021), metal–organic frameworks (MOFs) have attracted much attention in recent years in the fields of catalysis (Xu et al. 2019), adsorption (Liu et al. 2021), and light trapping (Lin et al. 2020; Kaur et al. 2020). In light of the limitations associated with conventional adsorbents—such as low selectivity, limited active sites, or difficulty in separation—there is a growing need for multifunctional materials capable of efficiently removing heavy metals from both simple and complex matrices. In this context, the present study introduces a novel hybrid adsorbent, CmBC-Fe_3O_4@ZnMOF, which integrates biochar (CmBC) with magnetic Fe_3O_4 nanoparticles and Zn-based metal–organic frameworks (ZnMOFs) containing pyridine ligands. This unique combination offers multiple adsorption mechanisms, including pore filling through

the biochar matrix and strong chemical interactions via –OH, –COOH, and nitrogen-containing functional groups. The incorporation of Fe_3O_4 provides magnetic separability, while ZnMOF enhances coordination-driven binding capacity. Such a synergistic design has rarely been reported in literature and is expected to provide enhanced performance in both selective and efficient removal of heavy metals, particularly in complex matrices, such as milk. This work thus presents a new-generation adsorbent platform for cost-effective, environmental, and food safety applications.

In this study, Fe_3O_4 activated magnetic BC (CmBC-Fe_3O_4) was synthesized by a one-step pyrolysis method as a low-cost, environmentally friendly, and porous carbon source with excellent adsorption properties. It was then modified with Zn(II)-based coordination polymer synthesized by solvothermal method to obtain hybrid material (CmBC-Fe_3O_4@ZnMOF) to increase the adsorption capacity by replacing the surface charge of BC with metal nanoparticles and to gain magnetic properties with respect to BC, MOF, and metal nanoparticles. The synthesized hybrid material were used as adsorbents for the removal of Mn(II), Cu(II), Cd(II), and Pb(II) from both synthetic water and milk samples by batch adsorption method for single and simultaneous (binary and quadruple competition) adsorption.

2 | Materials and Methods

2.1 | Chemicals and Reagents

Iron(II) sulfate heptahydrate ($FeSO_4{\cdot}7H_2O$), zinc acetate dihydrate ($Zn(CH_3CO_2)_2{\cdot}2H_2O$), Iron(III) chloride hexahydrate ($FeCl_3{\cdot}6H_2O$), 4,4′-bipyridine ($(C_5H_4N)_2$), dimethylformamide *(DMF*: $((CH_3)_2NC(O)H$), and trimesic acid ($C_6H_3(CO_2H)_3$) were obtained from Sigma-Aldrich. Pb(II), Cd(II), Cu(II), and Mn(II) standard solutions at 1000-mg/L concentration were supplied by Merck. Animal wastes to be used in BC production were obtained from the manure of cattle raised in the animal farm of Burdur Mehmet Akif Ersoy University. Packaged milk was obtained from markets in Burdur city, Turkey. Since all chemicals were of high purity, no pre-treatment was applied. Double-distilled water with a conductivity of 18.2 MΩ·cm was used throughout the experimental studies.

2.2 | Preparation of Fe_3O_4 Activated Magnetic Biochar (CmBC-Fe_3O_4)

The cow manure collected from the animal farm of Burdur Mehmet Akif Ersoy University was dried in an oven at 70°C for 48 h to remove dust and impurities from it prior to pyrolysis and then pulverized. In a 250-mL beaker, 9.0-g $FeCl_3{\cdot}6H_2O$ and 4.6-g $FeSO_4{\cdot}7H_2O$ were added and dissolved with 100-mL ultrapure water in an ultrasonic bath. Subsequently, 10.0 g of biomass was introduced into the mixture and stirred at room temperature for 30 min. Finally, the whole mixture was placed in a porcelain crucible with a lid and pyrolysed at 700°C in a muffle furnace to obtain CmBC-Fe_3O_4 magnetic composite by one-step in situ synthesis method. The pyrolysis process was carried out at 700°C and 4 h in a noncirculating air atmosphere. The obtained Fe_3O_4 activated magnetic BC (CmBC-Fe_3O_4) was thoroughly washed with double-distilled water until the pH reached a neutral value and dried at 85°C for 24 h and stored in a desiccator.

2.3 | Preparation of CmBC-Fe_3O_4@ZnMOF Hybrid Material

For the synthesis of CmBC-Fe_3O_4@ZnMOF, ZnMOF was firstly synthesized by solvothermal method. In the synthesis method, after preparing the metal–ligand solution, it was taken into a steel-protected Teflon reactor. The reactor was sealed and kept in an oven for 24–48 h. Afterward, the reactor removed from the oven is cooled to room temperature, the solution is separated by centrifugation, washed with the appropriate solvent, and dried to obtain the final MOF structures (Liu et al. 2021; Raut et al. 2021; Lin et al. 2020; Kaur et al. 2020; Maina et al. 2018); 20 mL of DMF:H_2O (4:1 ratio) including 1 mmol of $Zn(CH_3CO_2)_2{\cdot}2H_2O$, 1 mmol of $(C_5H_4N)_2$, and 0.5 mmol of $C_6H_3(CO_2H)_3$ was placed in 100-mL stainless steel autoclave lined with Teflon. The mixture was sonicated in an ultrasonic water bath for half an hour. The pH of the solution was raised to pH 4.2 using approximately 1.0-mL NaOH and stirred for a further 10 min. The reactor was placed in an oven heated from room temperature to 120°C for 12 h, kept at 120°C for 48 h, and then cooled to room temperature for 24 h. At the end of the synthesis, the ZnMOF crystals were filtered through blue-banded filter paper and washed several times with both double-distilled water and DMF. The crystals obtained after washing (yield ~80%, relative to Zn) were dried at 70°C for 10 h.

The CmBC-Fe_3O_4@ZnMOF hybrid material was synthesized by the hydrothermal impregnation strategy shown in Figure 1. The previously synthesized of both CmBC-Fe_3O_4 and ZnMOF were dispersed as a 1:2 ratios and ultrasonicated in 35 mL of DMF and 5 mL of H_2O for half an hour. The mixed solution was taken into a 100-mL stainless steel autoclave reactor and heated to 120°C for 12 h. After allowing it to cool at ambient temperature, the resulting yellowish-white precipitate was isolated by centrifugation and washed several times with DMF and double-distilled water. The obtained CmBC-Fe_3O_4@ZnMOF was dried in an oven at 80°C during overnight.

2.4 | Characterization of CmBC-Fe_3O_4, ZnMOF, and CmBC-Fe_3O_4@ZnMOF

Scanning electron microscopy equipped with energy dispersive X-ray spectrometry (SEM–EDX, Carl Zeiss EVO-LS 10, Jena, Germany), X-ray diffraction analysis (XRD, Bruker D8 Advance, Kα radiation with about 2θ: 10°–90°, Karlsruhe, Germany), Fourier transform infrared spectroscopy (FTIR, Perkin El Elmer Fronter, Massachusetts, USA), thermogravimetric and differential thermal analysis (SEIKO SII, TG/DTA 7200, Chiba, Japan), and N_2 adsorption–desorption isotherms (Quantachrome Quadrasorb SI, 77K, P/P0~ 0. 99, Florida, USA) were used to characterize the surface morphologies, elemental compositions, thermal stability, and chemical structures of the synthesized CmBC-Fe_3O_4, ZnMOF, and CmBC-Fe_3O_4@ZnMOF. Before analysis, the samples were dried in an oven at 105 °C for 24 h, followed by degassing in a vacuum

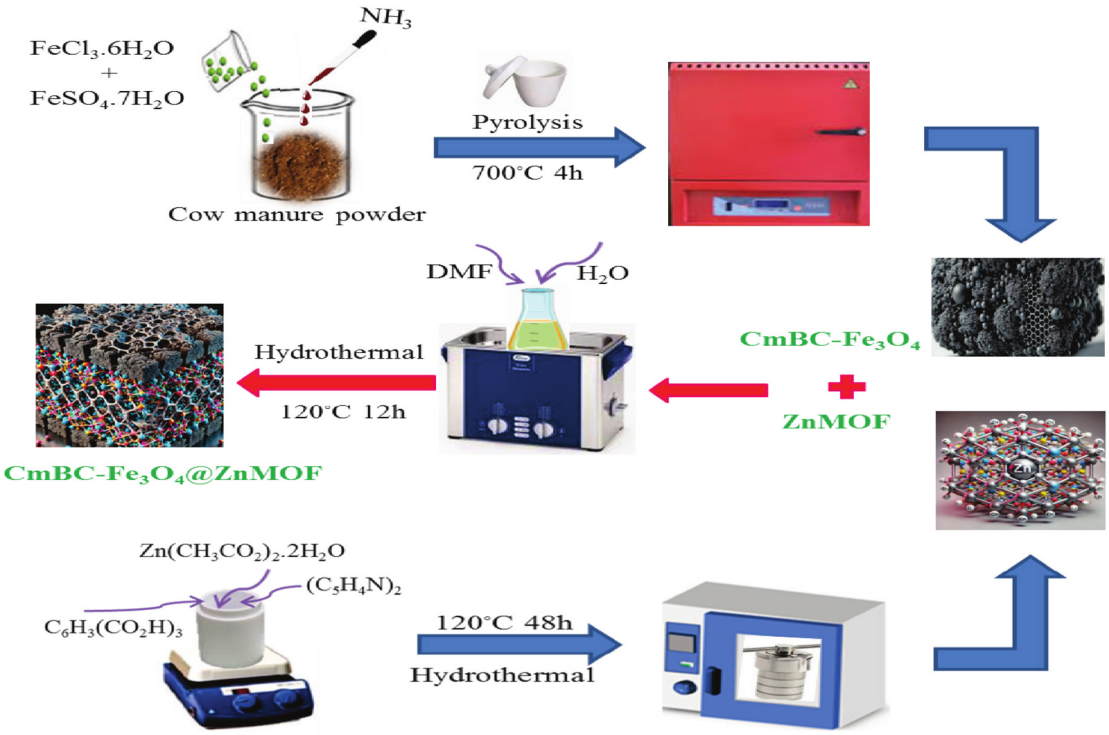

FIGURE 1 | Schematic representation of the synthesis method of CmBC-Fe_3O_4@ZnMOF hybrid material obtained from both CmBC-Fe_3O_4 and ZnMOF.

environment at 300°C for 5 h. Data obtained from the analyses were visualized with Origin Pro version 9 software (Origin Lab Corporation, Massachusetts, USA). The concentration of Cu(II), Pb(II), Mn(II), and Cd(II) in milk and synthetic water samples was determined with Agilent 240 model flame atom absorption spectrometer (FAAS, Waldbronn, Germany). The digestion of the milk sample was carried out in a CEM (Mars 6, Matthews, USA) brand microwave oven.

2.5 | Determination of Pb(II), Cd(II), Cu(II), and Mn(II) in Both Water and Milk Samples

Since the concentrations of Pb(II), Cd(II), Cu(II), and Mn(II) ions in double-distilled water were below the detection limits of the FAAS instrument, synthetic water solutions containing 10 mg/L of each metal ion were prepared and used in the adsorption experiments. On the other hand, the milk samples were prepared similar to the literature before batch adsorption (Lanjwani, Altunay, and Tuzen 2023; Kaynaker et al. 2018); 10 mL of the milk samples was carefully added to a centrifuge tube (15 mL) containing 1-mL (15%, w/v) trichloroacetic acid solution. The resulting mixture was then vortexed at 2500 rpm for 3 min and centrifuged at 3000 rpm for 10 min. The supernatant was filtered with 0.45-μm filter paper to remove denatured proteins and stored in the refrigerator at 4°C. To determine the concentrations of the heavy metals in milk samples, 1 mL of the milk sample was first placed in the Teflon sample containers in a microwave oven, and 4.0 mL of 65% HNO_3 and 2.0 mL of 30% hydrogen peroxide (H_2O_2) were added, and then the mixture was kept at 180°C and 270 bar for 15 min. At the end of the process, the Teflon containers were allowed to cool for 15 min, and concentrations of those heavy metals were determined again using FAAS instrument. As the concentrations of Pb(II), Cd(II), Cu(II), and Mn(II) ions in the milk samples were also below the detection limits of the FAAS instrument, enriched milk solutions containing 10 mg/L of each metal ion were prepared using the same procedure applied to the synthetic water solutions.

TABLE 1 | Levels of factors used in experimental design.

Variables	Symbol	Low (−)	Central point (0)	High (+)
pH	A	3	5	8
CmBC-Fe_3O_4@ ZnMOF amount (mg)	B	10	25	50
Initial Pb concentration (mg/L)	C	10	20	40
Contact time (h)	D	4	8	12

2.6 | Batch Adsorption Procedure

Twenty-five milliliters each of samples including 10 mg/L of Pb(II), Cd(II), Cu(II), and Mn(II) were added to 50-mL falcon tubes, and pH was adjusted to 5.5 (using HCl or NaOH). Then, 10 mg of adsorbent was added, and the solutions were shaken at 25°C at 150 rpm for 12 h. At the end of the time, the solutions were filtered, and that heavy metal concentrations were determined by FAAS measurements at fixed wavelengths of 217 nm (Pb), 228.8 nm (Cd), 279.5 nm (Mn), and 324.8 nm (Cu). A three

level (low, central point, and high) factorial design (Lanjwani, Khuhawar, et al. 2023) was drawn using four variables such as pH, CmBC-Fe_3O_4@ZnMOF amount, initial Pb(II) concentration, and contact time to optimize the variables with the adsorbent that gave the best results (Table 1). Fifteen experimental runs were performed to investigate the effects of each experiment on heavy metals and the effluents of each run were estimated (Table 2).

TABLE 2 | Experiments for factorial design.

Run	A	B	C	D	Removal (%)
1	−	+	−	+	68.50
2	+	−	−	−	20.00
3	−	−	+	−	52.54
4	+	+	−	+	25.12
5	0	0	0	+	85.45
6	+	−	+	0	23.07
7	−	−	0	−	46.68
8	+	+	0	−	18.75
9	−	+	−	−	45.00
10	0	0	0	0	83.23
11	+	−	+	+	15.27
12	−	0	0	0	73.75
13	0	0	+	0	85.78
14	0	+	+	0	87.14
15	0	0	−	+	81.43

3 | Results and Discussion

3.1 | Characterization Results

FTIR analysis (Figure 2a) was performed to detect the surface functional groups present in the composite material before and after adsorption. Furthermore, XRD analysis (Figure 2b) was also performed to confirm the identification of crystalline phases. The major functional groups present on the surface of the synthesized materials are given in Figure 2a. The FTIR spectrum of CmBC-Fe_3O_4 showed bands at approximately 3435 cm^{-1} (OH hydroxyl group in phenol and carboxylic groups), both 1465 and 1080 cm^{-1} (C-O vibrations of carbonate group) and 870 cm^{-1} (Fe-O bond), confirming that the biochar was activated by Fe_3O_4. The FTIR spectra of ZnMOF revealed the characteristic peaks of carboxylic acid and 4,4′-bipyridine coordination with Zn metal ions at 820 and 645 cm^{-1}, respectively. The observation of the same peaks in the FTIR spectrum of CmBC-Fe_3O_4@ZnMOF hybrid material confirmed the modification. It was also observed that the peaks were slightly shifted to the right after adsorption. Among the identified functional groups, carboxyl and hydroxyl groups are known to be polar and active groups that potentially play a crucial role in the adsorption process for heavy metals through outer sphere complexation (electrostatic attraction) and inner sphere complexation (nonelectrostatic attraction) (Tran et al. 2016).

Figure 2b shows the X-ray powder diffraction patterns of the three synthesized materials and the CmBC-Fe_3O_4@ZnMOF adsorbent before and after Pb(II) adsorption. In the XRD pattern of CmBC-Fe_3O_4, two broad diffraction peaks centered at $2\theta = 22^\circ$ and 43° corresponded to the (002) planes of graphite and the (100) reflections originating from the in-plane structure of graphitic crystallites (Bedin et al. 2018). According to the Fe_3O_4 JCPDS-ICDD database (PDF 19-0629), the corresponding positions (approximately $2\theta = 30^\circ$, 36°, 57°, and 62°) were identified with respect to the (220), (311), (511), and (440) crystal faces, respectively (Li et al. 2008). The presence of diffraction peaks

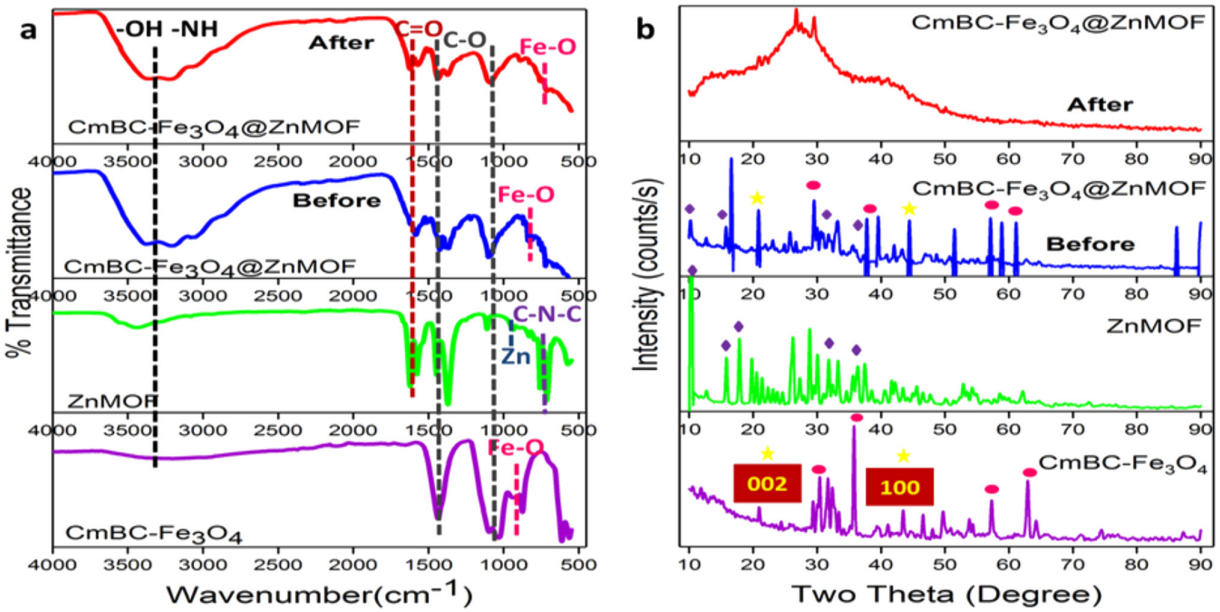

FIGURE 2 | (a) Comparative FTIR spectra and (b) XRD data of the prepared materials.

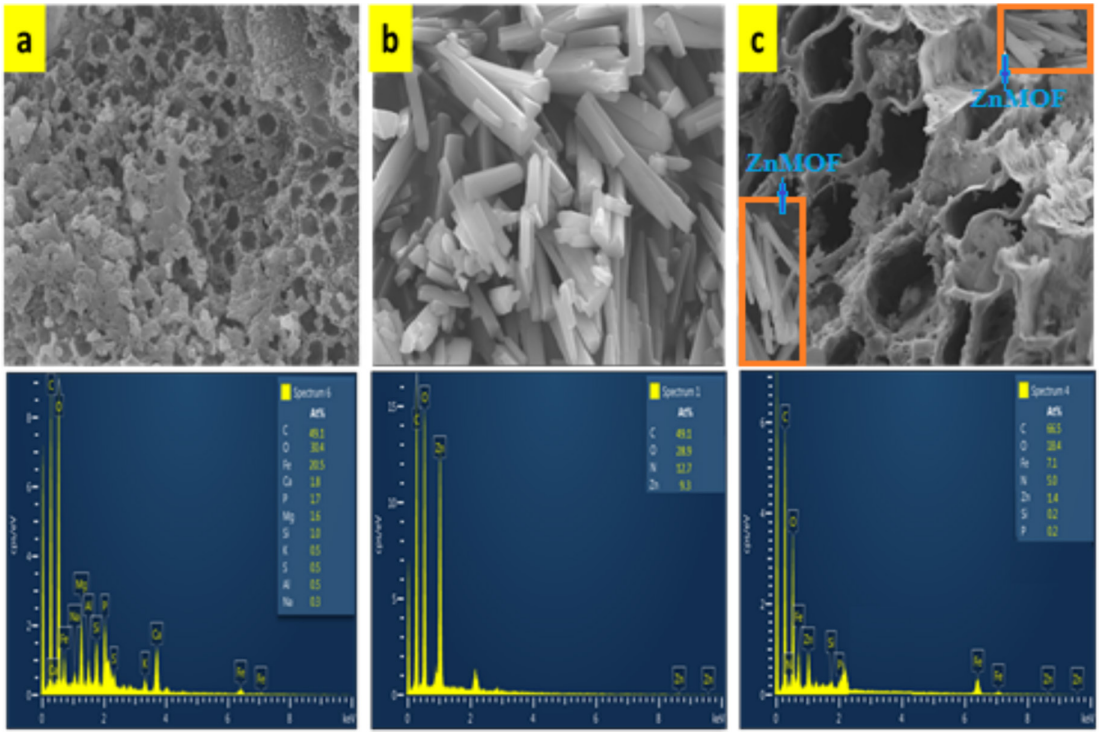

FIGURE 3 | SEM images and EDX analysis of (a) CmBC-Fe_3O_4, (b) ZnMOF, and (c) CmBC-Fe_3O_4@ZnMOF.

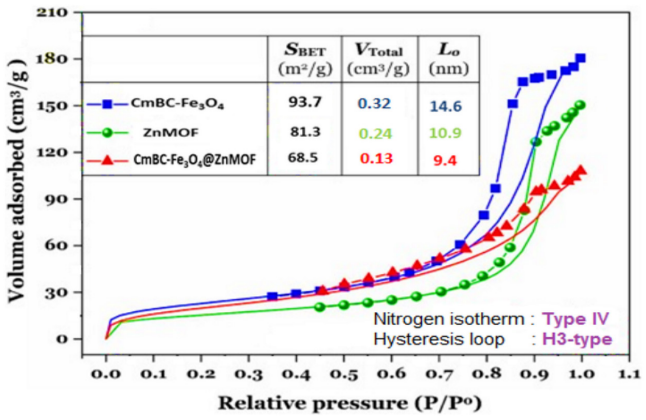

FIGURE 4 | Nitrogen adsorption/desorption isotherm of CmBC-Fe_3O_4, ZnMOF, and CmBC-Fe_3O_4@ZnMOF at 77.3 K.

at 10.57° and 13.27°, which are consistent with the literature on ZnMOF, are assigned to the (220) and (400) lattice planes, respectively (Sharma et al. 2021; Dang et al. 2020), suggesting that the ZnMOF was successfully prepared. The crystal size of ZnMOF was calculated and found to be 18.7 nm from the Scherrer equation. The average crystal sizes of both biochar and hybrid material were estimated as 23.1 and 27.4 nm, respectively, based on ZnMOF. The decrease in all diffraction peaks of the CmBC-Fe_3O_4@ZnMOF hybrid material after adsorption suggests that adsorption occurs on the entire surface and the crystal structure does not change (Z. Yang, Chen, et al. 2020; Rout et al. 2015).

The differences in surface morphology of the prepared materials are seen in Figure 3. SEM images were taken at a magnification of 15,000×, and the scale bar corresponds to 1 μm. Clearly, the Fe_3O_4 activated magnetic BC obtained from cow manure exhibited a nonspherical morphology with porous structure (Figure 3a) (Jing et al. 2018). EDX analysis showed that it was typical carbonaceous materials due to the non-spherical BC (77% C). This means that the BC can exhibit high hardness number (i.e., high mechanical strength) and high acidic stability (i.e., strong chemical stability). In addition, the presence of Fe in EDX analysis confirmed that it was activated, and the presence of other elements (such as Ca, Mg, P, and K) is also consistent with the XRD diffraction peaks. Figure 3b shows the SEM image of ZnMOF with rodlike crystals. The composition of ZnMOF was determined to consist of carbon, oxygen, nitrogen, and zinc with the ratios of 49.1, 28.9, 12.7, and 9.3, respectively, as shown in Figure 3b. Both EDX analysis and SEM images of CmBC-Fe_3O_4@ZnMOF (Figure 3c) confirm that the hybrid material was successfully synthesized.

The textural properties of the prepared CmBC-Fe_3O_4, ZnMOF and CmBC-Fe_3O_4@ZnMOF were investigated by nitrogen adsorption/desorption isotherm at 77.3 K (Figure 4). According to the IUPAC nomenclature, the physical adsorption isotherm of the whole material was categorized as type IV, where the H3-type hysteresis loop could be seen in the isotherms at a relative pressure (P/P_o) higher than 0.35. Moreover, the emergence of a wide range of the H3-type hysteresis loop at high P/P_o values (0.35–1.0) indicated that it consisted of narrow slit-like pores, and the material surface could be covered in multilayers (Yurdakal et al. 2019; Thommes et al. 2015). From the BET results, it was found that all the materials (2–50-nm range) were mesoporous. The large specific surface area (S_{BET}) followed the decreasing order: CmBC-Fe_3O_4 > ZnMOF > CmBC-Fe_3O_4@ZnMOF. It is thought that the porosity properties of CmBC-Fe_3O_4 decreased after the modification process with ZnMOF, probably due to the binding to the particle surface (Naeimi et al. 2015). In this case, it is predicted that the hybrid material can provide more binding points for heavy metal adsorption.

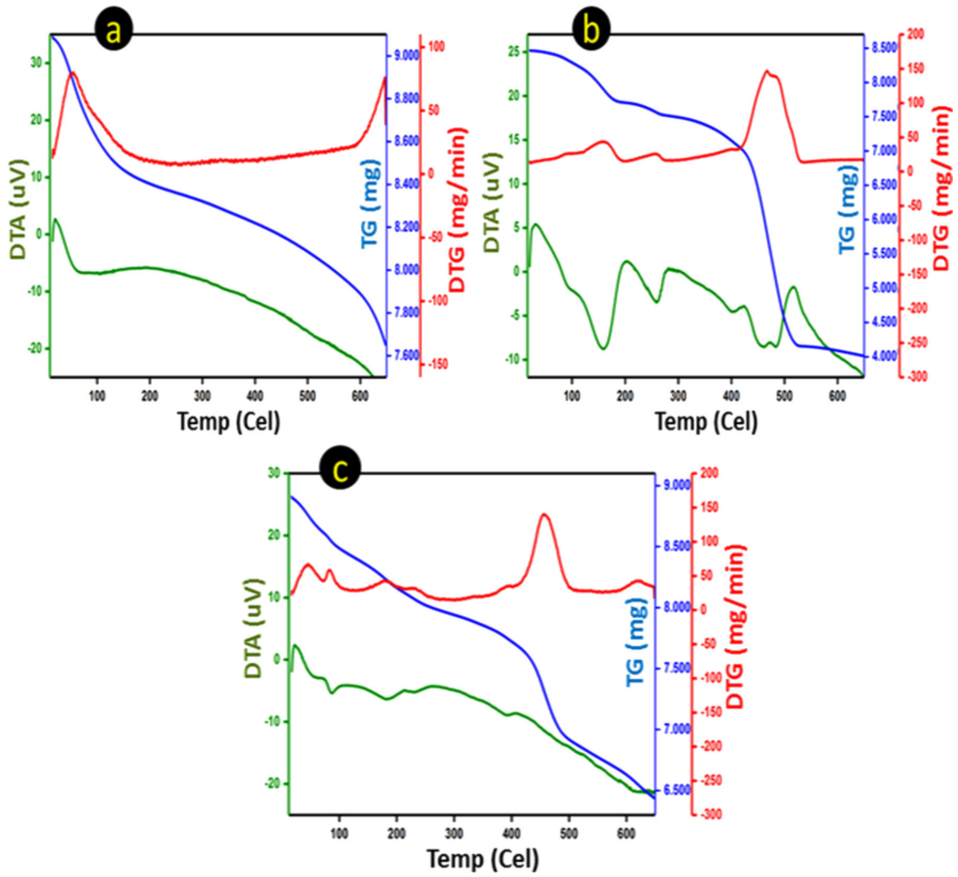

FIGURE 5 | DTA, DTG, and TG curves of (a) CmBC-Fe_3O_4, (b) ZnMOF, and (c) CmBC-Fe_3O_4@ZnMOF.

The DTA, DTG, and TG curves for comparing the thermal decomposition behaviors of the synthesized CmBC-Fe_3O_4, ZnMOF, and CmBC-Fe_3O_4@ZnMOF are given in Figure 5. According to TG and DTG curves of the CmBC-Fe_3O_4 (Figure 5a), a significant loss in the material mass occurs in two stages between 100°C–200°C and 300°C–500°C (5.2% and 16.5%, respectively). The mass loss in the first stage can generally be associated with the evaporation of surface moisture in the material or the loss of volatile compounds (Cao et al. 2021). The mass loss in the second stage is more pronounced, and it is seen that the main structure of the material begins to thermally decompose. This region generally represents the breakage of carbon chains for organic structures or the complete dissociation of the material structure (Cao et al. 2021). In other words, both semicarbonized organic structures and functional groups, such as carboxyl and carbonyl in CmBC-Fe_3O_4 are decomposed, which leads to the deterioration of both structural integrity and higher mass loss. The endothermic peak around 100°C in the DTA curve (Figure 5a) indicates that energy is taken during the removal of moisture. The exothermic peak seen in the range of 400°C–500°C indicates that energy is released during the decomposition of organic structures.

In TG curve of the ZnMOF (Figure 5b), mass loss occurs in three stages, and a more significant mass loss (around 38%) occurs in the second stage. It is thought that in this stage, the coordination bonds in the ZnMOF structures are weakened and the metal–ligand interactions are disrupted; and therefore, the organic ligands are dissociated. There is a small peak around 200°C in the DTG curve, and there is a significant peak in the range of 400°C–500°C in DTG curve. This peak indicates that the decomposition rate reaches its maximum at 400°C–500°C, and it is understood from the DTA curve that it is an exothermic process. In the third stage, the mass loss is the least (1.2%) above 500°C. It is observed from the DTG and TG curves of the hybrid material (Figure 5c) that there is a 3-stage mass loss. The DTG peak around 150°C is the point where the moisture loss rate is maximum. The pronounced DTG peak around 400°C indicates the temperature at which the main structural decomposition occurs. A smaller peak around 550°C may indicate additional reactions, inorganic compounds or residual substances. The DTA curve indicates that the first stage is endothermic, and the other stages at higher temperatures are exothermic processes. As a result, the presence of multiple decomposition peaks at lower temperatures in CmBC-Fe_3O_4 (Figure 5a) suggests that the material possesses a multilayered or structurally complex nature, which is consistent with the findings of the BET analysis.

3.2 | Heavy Metal Adsorption Studies

3.2.1 | Adsorption Performance

The adsorption studies of Pb(II), Cd(II), Mn(II), and Cu(II) with CmBC-Fe_3O_4, ZnMOF, and CmBC-Fe_3O_4@ZnMOF adsorbents from both synthetic water and milk samples, prepared as described in section "Determination of Pb(II), Cd(II), Cu(II), and Mn(II) in both water and milk samples," were carried out under

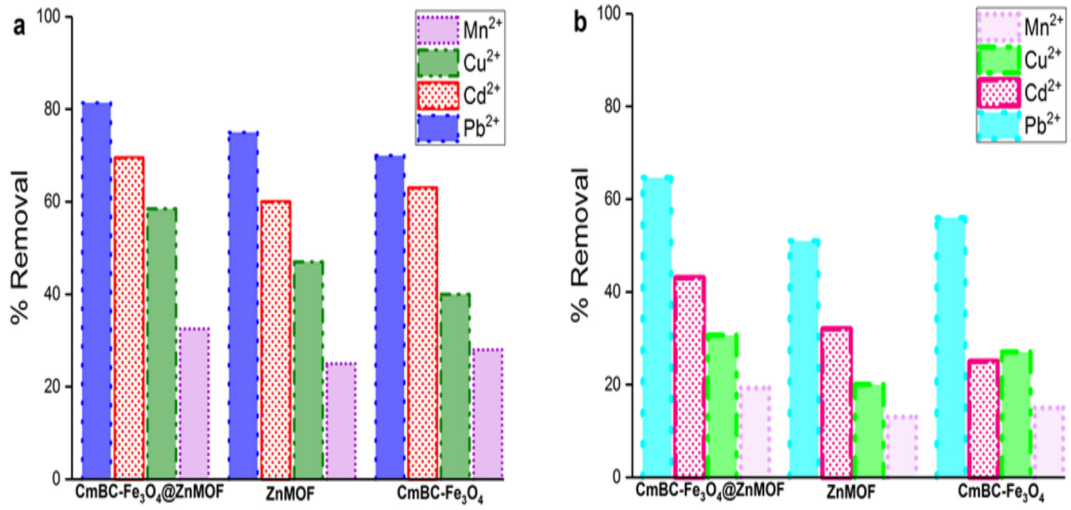

FIGURE 6 | Adsorption of Pb(II), Cd(II), Cu(II), and Mn(II) by various adsorbents in (a) aqueous phase and (b) milk (initial ion concentration: 10 mg/L, adsorbent dosage: 10 mg/25 mL, T = 298 K, pH = 5.5, and 12 h).

the experimental conditions described in section "Batch adsorption procedure." To evaluate the performance of the synthesized CmBC-Fe_3O_4@ZnMOF adsorbent, the control experiments were conducted using individual components including CmBC-Fe_3O_4 and ZnMOF. These controls allowed direct comparison of removal efficiencies, highlighting the synergistic effect and enhanced adsorption capacity of the hybrid material. To ensure comparability, these control adsorbents were subjected to identical experimental conditions, including the same initial metal ion concentrations, contact time, and pH. Adsorption studies show that the best adsorbent in heavy metal removal from both water and milk was found to be the CmBC-Fe_3O_4@ZnMOF hybrid material (Figure 6). According to the BET analysis results, the fact that CmBC-Fe_3O_4, which had the highest surface area and pore size, provided lower removal than the hybrid material, suggests that the sorption was in the form of interaction with functional groups rather than pore filling.

Based on Figure 6, the adsorption capacity of the hybrid material in both the synthetic water and milk samples was in the order of Pb(II) > Cd(II) > Cu(II) > Mn(II). Furthermore, the factorial design studies were carried out to determine the optimum conditions for the removal of Pb(II) using the hybrid adsorbent in synthetic water sample. In addition, competitive adsorption experiments and kinetic and isotherm studies were carried out in the synthetic water sample with the hybrid material under optimum conditions.

3.2.2 | Factorial Design

Factorial design offers a statistical experimental strategy that provides significant information about both important and trivial experimental variables, allowing for the analysis of large data sets with fewer experimental trials (Shanmugam et al. 2022). The 3D response surface plot of pH and the adsorbent dosage of CmBC-Fe_3O_4@ZnMOF (Figure 7a) indicates that the optimal response was achieved at pH 5 and an adsorbent dosage of 40 mg. The 3D surface plot of pH and initial Pb(II) concentration (Figure 7b) suggests that a better response was observed at pH 5 and an initial Pb concentration of 35 mg/L. The 3D response surface plot of pH and contact time (Figure 7c) shows that the most favorable response was observed at pH 5 and a contact time of 8 h. The 3D response plot of adsorbent dosage and contact time (Figure 7d) reveals that a good response was obtained at an adsorbent dosage of 40 mg and a contact time of 8 h, with the equilibrium time for Pb removal being approximately 8 h, after which the removal efficiency does not significantly change. The 3D surface plot of adsorbent dosage versus initial Pb(II) concentration (Figure 7e) demonstrates that the highest response occurred with an adsorbent dosage of 40 mg and an initial Pb concentration of 35 mg/L. The 3D surface plot (Figure 7f) of initial Pb(II) concentration versus contact time indicates that there was no direct correlation between these two parameters.

The Pareto chart shows the standardized and unstandardized effects of the parameters used for Pb(II) removal, with the tallest column representing the most statistically significant factors, while the shorter columns indicate the less significant effects of the variables (Rashad et al. 2023). The Pareto chart further reveals that variables A (pH), B (CmBC-Fe_3O_4@ZnMOF amount), C (initial Pb(II) concentration), and the combined factors AB and AC exceed the critical threshold and exhibit significant effects (Figure 8). In contrast, variables D, AD, BC, BD, and CD were found to be insignificant, as they fall below the reference line.

3.2.3 | Adsorption Isotherms and Kinetics

In order to define the adsorption constants and explain the interactions between the adsorbate and the adsorbent, the equilibrium data were analyzed with Dubinin–Radushkevich (D-R), Freundlich, and Langmuir isotherm models (Figure 9a). Adsorption kinetic studies were carried out at 298 K for 2–60 min. All adsorption isotherm experiments were carried out at 298 K at pH 5 for 8 h with target metal initial concentrations in the range of 2.5 to 200 mg/L. In order to minimize the modeling errors, the model was modeled with nonlinear optimization technique using Origin program (Tran et al. 2017). From the results (Table 3), it is seen that the Freundlich model generally

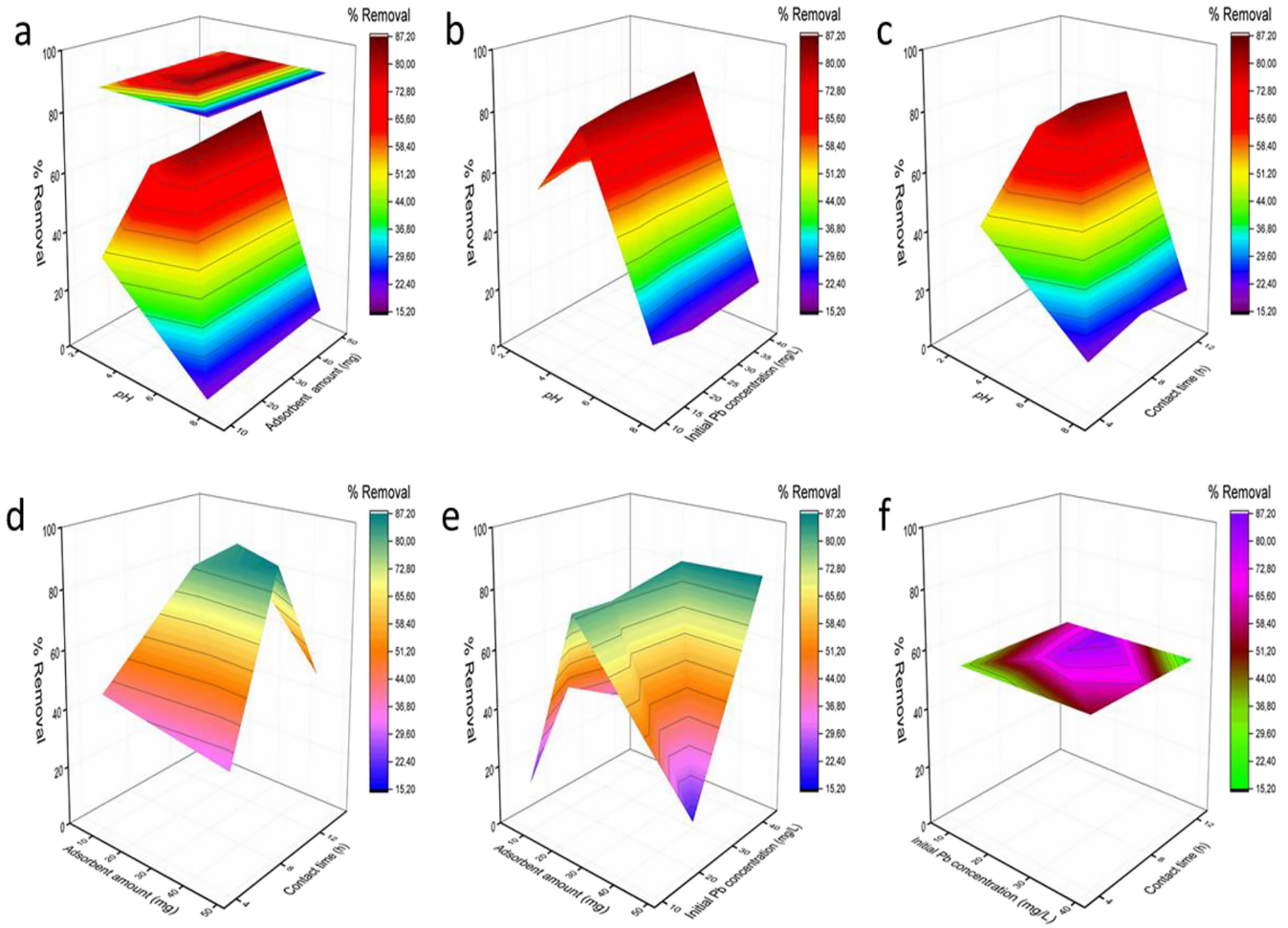

FIGURE 7 | The 3D plots of (a) pH with adsorbent amount, (b) pH with initial Pb (II) concentration, (c) pH with contact time, (d) adsorbent amount with contact time, (e) adsorbent amount with initial Pb(II) concentration, and (f) initial Pb(II) concentration with contact time versus for removal%.

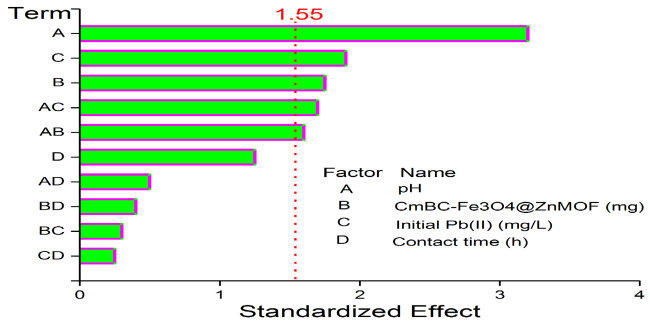

FIGURE 8 | Pareto chart of variables.

explained the isotherm better than the Dubinin–Radushkevich and Langmuir models.

Adsorption kinetic studies were carried out at 298 K for 2–480 min (Figure 9b). The adsorption process on magnetic BC and ZnMOF based hybrid adsorbent was very fast in the first 60 min. More than 50% of the heavy metals in the solution were adsorbed within approximately the first 60 min of contact time. This suggests that the synthesized magnetic hybrid material has a strong affinity for cations in the water environment. In general, the adsorption process increased successively during the initial 60 min contact time and then plateaued after approximately 180 min, but measurements continued for up to 8 h for Mn(II) to reach equilibrium. In this study, the nonlinear forms of Elovich, pseudo-second-order (PSO) and pseudo-first-order (PFO) kinetic models were chosen to describe the intrinsic adsorption constants. The kinetic data regarding adsorption were described more appropriately by the PSO model than both the PFO and Elovich models (Table 3).

One of the most critical points for adsorbents is their reusability. In order to investigate the reusability of the CmBC-Fe_3O_4@ZnMOF adsorbent, adsorption/desorption studies were repeated as three times. As seen in Figure 10, the adsorbent has an active and stable structure with a minor decline in adsorption capacity. The desorption process was carried out using ethanol, which is cheap and does not have a destructive effect on the adsorbent. The reusability results and the FTIR and XRD results after adsorption (Figure 2) confirmed the heavy metal removal ability of the prepared magnetic hybrid adsorbent.

The environmental wastewater is inherently complex, making it essential to study the adsorption behavior of various metal ions on CmBC-Fe_3O_4@ZnMOF under environmental conditions. To investigate this, competitive adsorption experiments were conducted involving binary or quadruple metal ions simultaneously in synthetic water sample. The results were compared to the

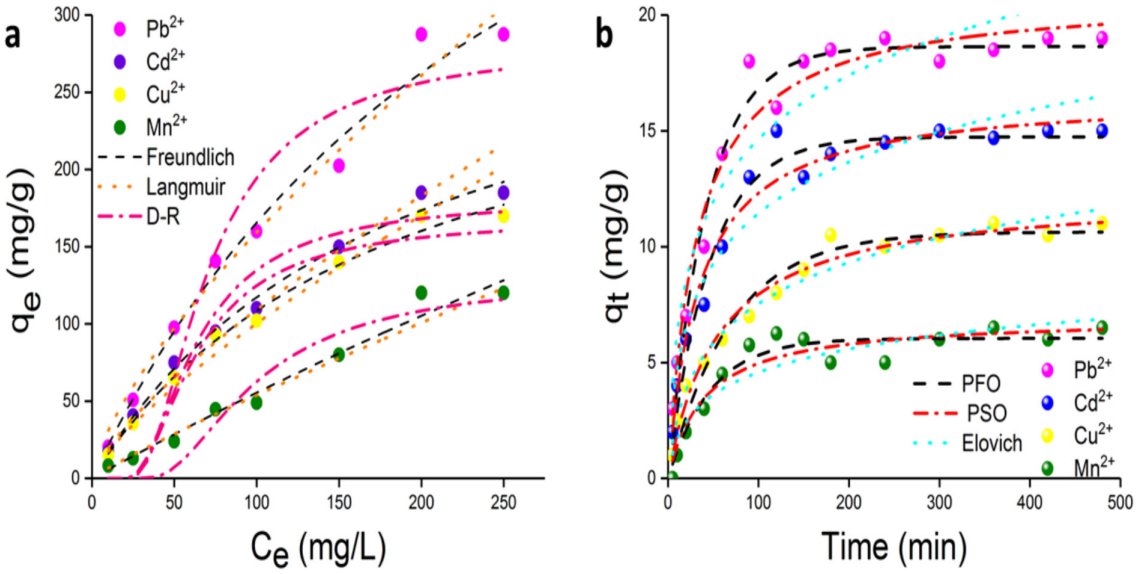

FIGURE 9 | (a) Isotherm and (b) kinetic models for the adsorption of Pb(II), Cd(II), Cu(II), and Mn(II) onto CmBC-Fe_3O_4@ZnMOF.

TABLE 3 | Kinetic and Isotherm model constants for the adsorption of some heavy metals on CmBC-Fe_3O_4@ZnMOF.

Kinetic/isotherm model parameters		Pb(II)	Cd(II)	Cu(II)	Mn(II)
PFO	q_e (mg/g)	18.643	14.741	10.641	6.044
	$k_1 * 10^{-3}$ (1/min)	2.331	2.171	1.442	2.124
	R^2	0.9675	0.9685	0.9790	0.9179
PSO	q_e (mg/g)	20.909	16.598	12.320	6.955
	$k_2 * 10^{-3}$ (g/mg*min)	1148	1.730	1.482	3.581
	R^2	0.9875	0.9839	0.9725	0.9454
Elovich	β (mg/g)	0.247	0.305	0.372	0.667
	α (g/mg*min)	1.467	1.044	0.419	0.303
	R^2	0.9066	0.9192	0.9713	0.8544
Langmuir	q_m (mg/g)	281.161	181.104	168.049	130.431
	K_L (L/mg)	3.724	2.978	3.006	7.413
	R^2	0.8862	0.8759	0.8972	0.9195
Freundlich	K_F (mg/g)/(mg/L)^n	3.426	3.549	2.979	0.837
	1/n	0.828	0.744	0.763	0.904
	R^2	0.9840	0.9909	0.9913	0.9743
Dubinin–Radushkevizch (D-R)	q_m (mg/g)	232.630	133.833	106.602	81.285
	K_{DR} (mol/kJ)^2	3.724	2.978	3.006	7.413
	R^2	0.8862	0.8759	0.8972	0.9195

adsorption capacities observed when each metal ion was present individually (as illustrated in Figure 11). During the experiments, the concentration of each metal ion was maintained at 10 mg/L, with 25 mg of CmBC-Fe_3O_4@ZnMOF dispersed in a 25-mL solution at room temperature for 8 h. As shown in Figure 11, the binary competitive adsorption (BCA) tests revealed that CmBC-Fe_3O_4@ZnMOF exhibits a consistent adsorption rate for Pb(II) ions, even in the presence of other metal ions, indicating that there is no interference effect from these ions. This behavior demonstrates the selective adsorption of Pb(II) by CmBC-Fe_3O_4@ZnMOF. A similar trend was also observed for Cd(II) ions; however, Pb(II) ions were found to slightly interfere with Cd(II) adsorption. In contrast, the adsorption efficiency of CmBC-Fe_3O_4@ZnMOF for Cu(II) and Mn(II) ions was significantly affected by the presence of all other metal ions, with Pb(II) ions exerting the most substantial inhibitory effect. These findings supported by both binary and

quaternary competitive adsorption (QCA) studies confirm that CmBC-Fe_3O_4@ZnMOF exhibits a higher selectivity for Pb(II) and Cd(II) ions compared to Cu(II) and Mn(II) ions in the competitive environments. Pb(II) and Cd(II) ions have relatively larger ionic radius and lower hydration energies than Cu(II) and Mn(II) ions, which facilitate their easier dehydration and subsequent coordination with the active sites on the adsorbent surface. In addition, FTIR analysis before and after adsorption (Figure 2a) shows distinct shifts and intensity changes in the bands corresponding to -COOH, -OH, and -C=O functional groups, suggesting their participation in complexation reactions. ZnMOF exhibits strong metal–ligand coordination through unsaturated metal sites and electron-rich functional moieties. These interactions probably contribute to the selective removal of Pb(II) and Cd(II) ions. The competitive adsorption studies with milk sample were also found to yield the same selectivity results; however, the adsorption capacity for metal ions was lower. This is thought to be due to both fat and proteins in the milk.

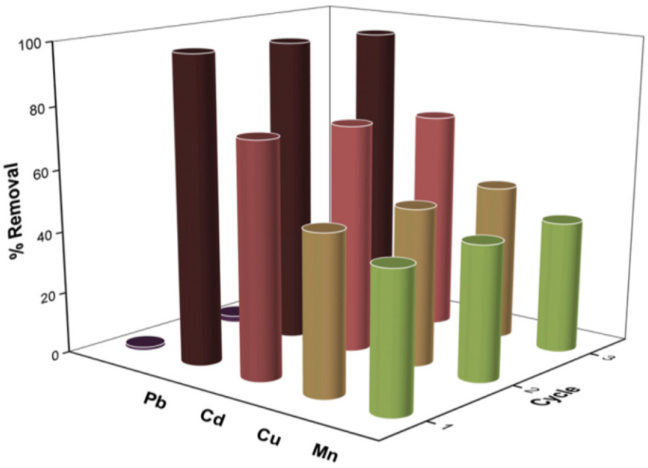

FIGURE 10 | Effect of three adsorption/desorption cycles on the percentage removal of Pb(II), Mn(II), Cd(II), and Cu(II).

3.3 | Adsorption Mechanism

CmBC-Fe_3O_4@ZnMOF hybrid adsorbent provides effective removal of heavy metal ions (Cu^{2+}, Cd^{2+}, Pb^{2+}, and Mn^{2+}) from aqueous media thanks to the multifaceted interaction mechanisms given in Figure 12.

In this hybrid structure, three basic components can undertake different tasks:

1. The functional groups (–COOH, –OH, C=O, aromatic π bonds) contained in CmBC-Fe_3O_4 can interact with metal ions via coordination bonds and electrostatic attraction paths. In addition, adsorption can also occur via pore diffusion thanks to the high surface area.
2. Hydrogen bonds and weak electrostatic interactions can occur between –OH groups on the Fe_3O_4 nanoparticle surface and heavy metal ions.
3. The porous structure of ZnMOF can directly bind metal ions thanks to the Zn^{2+} coordination centers on the inner surface and the nitrogen atoms in the 4,4′-bipyridine ligand.

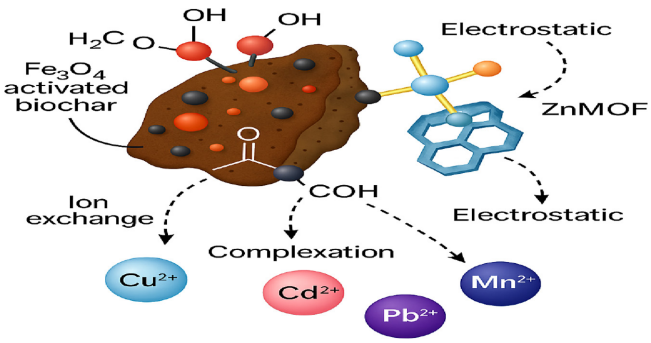

FIGURE 12 | Schematic representation of the adsorption mechanism of Cu^{2+}, Pb^{2+}, Cd^{2+}, and Mn^{2+} ions on the CmBC-Fe_3O_4@ZnMOF.

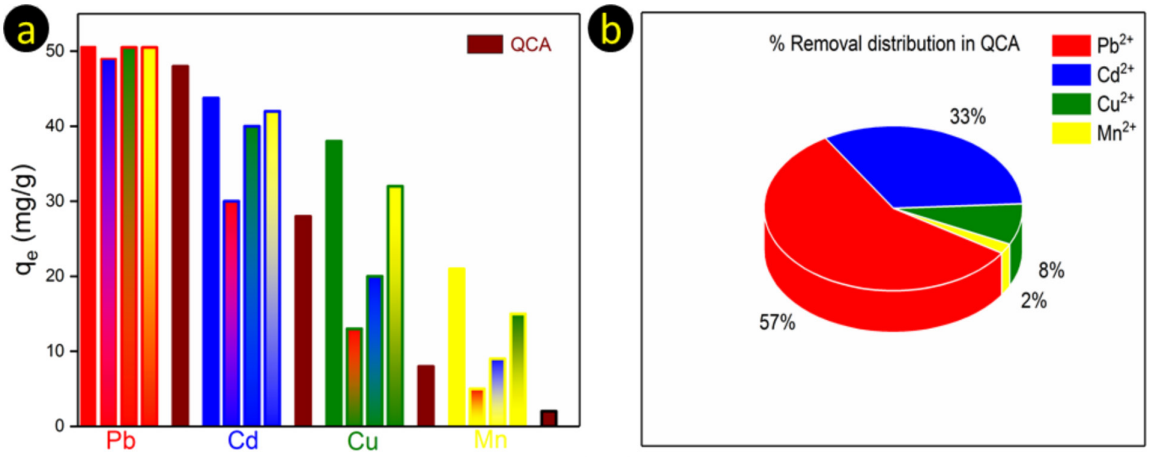

FIGURE 11 | (a) Comparison of Pb(II), Cd(II), Cu(II), and Mn(II) for binary and quadruple competitive adsorption capacities and (b) percent removal distribution in quadruple comparative adsorption.

In summary, thanks to the synergistic effect of this multicomponent hybrid structure, the adsorption mechanism occurs through the following pathways:

- √ Surface complexation (metal ion–functional group coordination).
- √ Ion exchange (especially $Cd^{2+} \leftrightarrow H^{+}$).
- √ π–ion interactions (for large ions such as Pb^{2+}).
- √ Electrostatic attraction.
- √ Pore diffusion and trapping of metal ions in MOF cavities.

4 | Conclusions

In the series of experiments, the removal of Cd(II), Pb(II), Mn(II), and Cu(II) ions from both synthetic water and milk samples using CmBC-Fe_3O_4, ZnMOF, and CmBC-Fe_3O_4@ZnMOF adsorbents was investigated in detail by single and competitive (binary and quaternary) adsorption techniques. Based on BET results, it was found that all the materials (2–50-nm range) were mesoporous, and CmBC-Fe_3O_4@ZnMOF has the lowest specific surface area (S_{BET}) because the porosity properties of CmBC-Fe_3O_4 decreased after modified with ZnMOF. Despite its lowest surface area, its highighst adsorption performance indicates that interactions with the functional groups on the surface are effective rather than pore filling. Its highights selectivity, especially for Pb(II) and Cd(II) ions, reveals that this material is a preferable adsorbent even in the complex sample matrices. Moreover, the model fits in line with kinetic and isotherm data also support these findings. This study clearly demonstrates the potential of the CmBC-Fe_3O_4@ZnMOF hybrid structure in the removal of heavy metal ions. In the future, the applicability of this hybrid structure should be further explored in more complex food matrices and environmental media, by enhancing it with different types of ZnMOFs, organic ligand modifications, or magnetic recovery strategies.

Author Contributions

Muradiye Şahin: methodology, funding acquisition, investigation, data curation, project administration, formal analysis, conceptualization, writing – original draft, writing – review, and editing. **Yasin Arslan:** validation, software, supervision, resources, project administration, methodology, investigation, funding acquisition, formal analysis, conceptualization, writing – original draft, writing – review, and editing. **Muhammet Atasoy:** methodology, investigation, data curation, formal analysis, conceptualization, and writing – original draft. **Mika Sillanpää:** visualization, validation, software, resources, methodology, investigation, formal analysis, conceptualization, writing – original draft, writing – review, and editing.

Acknowledgments

This study was supported by TUBITAK (The Scientific and Technological Research Council of Turkey) 2218 Project (122C199). Open access funding provided by the Scientific and Technological Research Council of Türkiye (TÜBİTAK). The authors wish to thank Kırşehir Ahi Evran University.

Conflicts of Interest

The authors declare no conflicts of interest.

Data Availability Statement

The data that support the findings of this study are available from the corresponding authors upon reasonable request.

References

Adenuga, A. A., O. D. Amos, J. A. O. Oyekunle, and E. H. Umukoro. 2019. "Adsorption Performance and Mechanism of a Low-Cost Biosorbent From Spent Seedcake of Calophyllum Inophyllum in Simultaneous Cleanup of Potentially Toxic Metals From Industrial Wastewater." *Journal of Environmental Chemical Engineering* 7: 103317.

Aziam, R., D. S. Stefan, S. Nouaa, M. Chiban, and M. Boşomoiu. 2024. "Adsorption of Metal Ions From Single and Binary Aqueous Systems on Bio-Nanocomposite, Alginate-Clay." *Nanomaterials (Basel)* 14, no. 4: 362.

Bedin, K. C., A. L. Cazetta, I. P. A. F. Souza, et al. 2018. "Porosity Enhancement of Spherical Activated Carbon: Influence and Optimization of Hydrothermal Synthesis Conditions Using Response Surface Methodology." *Journal of Environmental Chemical Engineering* 6: 991–999.

Cao, X., J. Zhang, K. Cen, F. Chen, D. Chen, and Y. Li. 2021. "Investigation of the Relevance Between Thermal Degradation Behavior and Physicochemical Property of Cellulose Under Different Torrefaction Severities." *Biomass and Bioenergy* 148: 106061.

Chen, G., C. Wang, J. Tian, et al. 2020. "Investigation on Cadmium Ions Removal From Water by Different Raw Materials-Derived Biochars." *Journal of Water Process Engineering* 35: 101223.

Chen, Q., J. Qin, Z. Cheng, et al. 2018. "Synthesis of a Stable Magnesium-Impregnated Biochar and Its Reduction of Phosphorus Leaching From Soil." *Chemosphere* 199: 402–408.

Chen, Q., J. Qin, P. Sun, Z. Cheng, and G. Shen. 2018. "Cow Dung-Derived Engineered Biochar for Reclaiming Phosphate From Aqueous Solution and Its Validation as Slow-Release Fertilizer in Soil-Crop System." *Journal of Cleaner Production* 172: 2009–2018.

Chen, Z., K. O. Kirlikovali, P. Li, and O. K. Farha. 2022. "Reticular Chemistry for Highly Porous Metal-Organic Frameworks: The Chemistry and Applications." *Accounts of Chemical Research* 55, no. 4: 579–591.

Dang, Y. T., M.-H. D. Dang, N. X. D. Mai, et al. 2020. "Room Temperature Synthesis of Biocompatible Nano Zn-MOF for the Rapid and Selective Adsorption of Curcumin." *Journal of Science: Advanced Materials and Devices* 5, no. 4: 560–565.

El-Dib, F. I., D. E. Mohamed, O. A. A. El-Shamy, and M. R. Mishrif. 2020. "Study the Adsorption Properties of Magnetite Nanoparticles in the Presence of Different Synthesized Surfactants for Heavy Metal Ions Removal." *Egyptian Journal of Petroleum* 29: 1–7.

Fato, F. T., D.-W. Li, L.-J. Zhao, K. Qiu, and Y.-T. Long. 2019. "Simultaneous Removal of Multiple Heavy Metal Ions From River Water Using Ultrafine Mesoporous Magnetite Nanoparticles." *ACS Omega* 4: 7543–7549.

Feizi, R., F. Hamidi, N. Jaafarzadeh, M. Ghahrchi, and A. Zafarzadeh. 2022. "Determination and Health Risk Assessment of Heavy Metals (Pb, Cd, Cu and Zn) in Different Brands of Pasteurized Milk." *International Journal of Environmental Analytical Chemistry* 102, no. 18: 6892–6903.

Hayati, B., A. Malekia, F. Najafi, et al. 2018. "Heavy Metal Adsorption Using PAMAM/CNT Nanocomposite From Aqueous Solution in Batch and Continuous Fixed Bed Systems." *Chemical Engineering Journal* 346: 258–270.

Jing, F., S. P. Sohi, Y. Liu, and J. Chen. 2018. "Insight Into Mechanism of Aged Biochar for Adsorption of PAEs: Reciprocal Effects of Ageing and Coexisting Cd^{2+}." *Environmental Pollution* 242: 1098–1107.

Jose, S. 2009. "Agroforestry for Ecosystem Services and Environmental Benefits: An Overview." *Agroforestry Systems* 76: 1–10.

Jungbluth, T., E. Hartung, and G. Brose. 2001. "Greenhouse Gas Emissions From Animal Houses and Manure Stores." *Nutrient Cycling in Agroecosystems* 60: 133–145.

Kaur, M., S. K. Mehta, and S. K. Kansal. 2020. "Amine-Functionalized Titanium Metal-Organic Framework (NH_2-MIL-125(Ti)): A Novel Fluorescent Sensor for the Highly Selective Sensing of Copper Ions." *Materials Chemistry and Physics* 254: 123539.

Kaynaker, M., M. Antep, and M. Merdivan. 2018. "Determination of Tetracyclines in Milk, Eggs and Honey Using In-Situ Ionic Liquid Based Dispersive Liquid-Liquid Microextraction." *Journal of Analytical Chemistry* 73, no. 1: 23–29.

Khalfa, L., A. Sdiri, M. Bagane, and M. L. Cervera. 2021. "A Calcined Clay Fixed Bed Adsorption Studies for the Removal of Heavy Metals From Aqueous Solutions." *Journal of Cleaner Production* 278: 123935.

Kharel, G., O. Sacko, X. Feng, et al. 2019. "Biochar Surface Oxygenation by Ozonization for Super High Cation Exchange Capacity." *ACS Sustainable Chemistry & Engineering* 7: 16410–16418.

Kumar, P. S., C. Senthamarai, A. S. L. Sai Deepthi, and R. Bharani. 2013. "Adsorption Isotherms, Kinetics and Mechanism of Pb(II) Ions Removal From Aqueous Solution Using Chemically Modified Agricultural Waste." *Canadian Journal of Chemical Engineering* 91: 1950–1956.

Lanjwani, M. F., N. Altunay, and M. Tuzen. 2023. "Preparation of Fatty Acid-Based Ternary Deep Eutectic Solvents: Application for Determination of Tetracycline Residue in Water, Honey and Milk Samples by Using Vortex-Assisted Microextraction." *Food Chemistry* 400: 134085.

Lanjwani, M. F., M. Y. Khuhawar, T. M. J. Khuhawar, et al. 2023. "Photocatalytic Degradation of Eriochrome Black T Dye by ZnO Nanoparticles Using Multivariate Factorial, Kinetics and Isotherm Models." *Journal of Cluster Science* 34: 1121–1132.

Lebron, Y. A. R., V. R. Moreira, G. P. Drumond, et al. 2020. "Graphene Oxide for Efficient Treatment of Real Contaminated Water by Mining Tailings: Metal Adsorption Studies to Paraopeba River and Risk Assessment." *Chemical Engineering Journal Advances* 2: 100017.

Li, G. Y., Y. R. Jiang, K. L. Huang, P. Ding, and J. Chen. 2008. "Preparation and Properties of Magnetic Fe_3O_4-Chitosan Nanoparticles." *Journal of Alloys and Compounds* 466: 451–456.

Li, J., N. Akdeniz, H. H. M. Kim, R. S. Gates, X. Wang, and K. Wang. 2021. "Quantification of Sustainable Animal Manure Utilization Strategies in Hangzhou, China." *Agricultural Systems* 191: 103150.

Li, R., J. J. Wang, L. A. Gaston, et al. 2018. "An Overview of Carbothermal Synthesis of Metal-Biochar Composites for the Removal of Oxyanion Contaminants From Aqueous Solution." *Carbon* 129: 674–687.

Lin, C., Z. Zou, Z. Lei, L. Wang, and Y. Song. 2020. "Fluorescent Metal-Organic Frameworks MIL-101(Al)-NH_2 for Rapid and Sensitive Detection of Ellagic Acid." *Spectrochimica Acta, Part A: Molecular and Biomolecular Spectroscopy* 242: 118739.

Liu, C., J. Wang, J. Wan, and C. Yu. 2021. "MOF-on-MOF Hybrids: Synthesis and Applications." *Coordination Chemistry Reviews* 432: 213743.

Liu, X., B. Jiang, X. Yin, H. Ma, and B. S. Hsiao. 2020. "Highly Permeable Nanofibrous Composite Microfiltration Membranes for Removal of Nanoparticles and Heavy Metal Ions." *Separation and Purification Technology* 233: 115976.

Maina, J. W., C. P. Gonzalo, A. Merenda, L. Kong, J. A. Schütz, and L. F. Dumée. 2018. "The Growth of High Density Network of MOF Nano-Crystals Across Macroporous Metal Substrates—Solvothermal Synthesis Versus Rapid Thermal Deposition." *Applied Surface Science* 427: 401–408.

Mondol, M. H., and S. H. Jhung. 2021. "Adsorptive Removal of Pesticides From Water With Metal-Organic Framework-Based Materials." *Chemical Engineering Journal* 421: 129688.

Naeimi, H., Z. S. Nazifi, and S. M. Amininezhad. 2015. "Preparation of Fe_3O_4 Encapsulated-Silica Sulfonic Acid Nanoparticles and Study of Their In Vitro Antimicrobial Activity." *Journal of Photochemistry and Photobiology B* 149: 180–188.

Ogamba, E. N., E. E. Charles, and S. C. Izah. 2021. "Distributions, Pollution Evaluation and Health Risk of Selected Heavy Metal in Surface Water of Taylor Creek, Bayelsa State, Nigeria." *Toxicology and Environmental Health Sciences* 13: 109–121.

Peng, H., P. Gao, G. Chu, B. Pan, J. Peng, and B. Xing. 2017. "Enhanced Adsorption of Cu(II) and Cd(II) by Phosphoric Acid-Modified Biochars." *Environmental Pollution* 229: 846–853.

Qin, J., Y. Cheng, M. Sun, L. Yan, and G. Shen. 2016. "Catalytic Degradation of the Soil Fumigant 1,3-Dichloropropene in Aqueous Biochar Slurry." *Science of the Total Environment* 569-570: 1–8.

Rashad, S., G. El-Chaghaby, E. C. Lima, and G. S. dos reis. 2023. "Optimizing the Ultrasonic-Assisted Extraction of Antioxidants From *Ulva lactuca* Algal Biomass Using Factorial Design." *Biomass Conversion and Biorefinery* 13: 5681–5690.

Raut, V., R. R. Wani, H. K. Chaudhari, and D. Das. 2021. "Solvent-Free One Pot Synthesis of 1,2-Dihydroquinolines From Anilines and Acetone Catalysed by MOF-199." *Results in Chemistry* 3: 100097.

Ren, S., C. Song, S. Ye, C. Cheng, and P. Gao. 2022. "The Spatiotemporal Variation in Heavy Metals in China's Farmland Soil Over the Past 20 Years: A Meta-Analysis." *Science of the Total Environment* 806: 150322.

Rockström, J., W. Steffen, K. Noone, et al. 2009. "A Safe Operating Space for Humanity." *Nature* 461: 472–475.

Rout, P. R., P. Bhunia, and R. R. Dash. 2015. "A Mechanistic Approach to Evaluate the Effectiveness of Red Soil as a Natural Adsorbent for Phosphate Removal From Wastewater." *Desalination and Water Treatment* 54, no. 2: 358–373.

Şahin, M., and Y. Arslan. 2023a. "Green Synthesis of Metal Nanoparticles and Magnetic Nanocomposites for Adsorption, Desorption and Preconcentration of Pb (II)." *ChemistrySelect* 8, no. 18: e202300708.

Şahin, M., and Y. Arslan. 2023b. "Adsorptive and Oxidative Removal of Naproxen and Diclofenac Using Ag NPs, Cu NPs and Ag/Cu NPs." *Research on Chemical Intermediates* 49: 3627–3643.

Şahin, M., Y. Arslan, and F. Tomul. 2024. "Adsorption, Oxidation, Kinetic and Thermodynamic Studies of Methyl Orange by Magnetic Fe_3O_4 NPs and Their Chitosan/Alginate Nanocomposites." *International Journal of Environmental Analytical Chemistry* 104, no. 18: 6254–6273.

Şahin, M., M. Atasoy, Y. Arslan, and D. Yıldız. 2023. "Removal of Ni (II), Cu (II), Pb (II), and Cd (II) From Aqueous Phases by Silver Nanoparticles and Magnetic Nanoparticles/Nanocomposites." *ACS Omega* 8: 34834–34843.

Semerjian, L. 2018. "Removal of Heavy Metals (Cu, Pb) From Aqueous Solutions Using Pine (Pinus Halepensis) Sawdust: Equilibrium, Kinetic, and Thermodynamic Studies." *Environmental Technology & Innovation* 12: 91–103.

Shahrashoub, M., and S. Bakhtiari. 2021. "The Efficiency of Activated Carbon/Magnetite Nanoparticles Composites in Copper Removal: Industrial Waste Recovery, Green Synthesis, Characterization, and Adsorption-Desorption Studies." *Microporous and Mesoporous Materials* 311: 110692.

Shan, R., Y. Shi, J. Gu, Y. Wang, and H. Yuan. 2020. "Single and Competitive Adsorption Affinity of Heavy Metals Toward Peanut Shell-Derived Biochar and Its Mechanisms in Aqueous Systems." *Chinese Journal of Chemical Engineering* 28: 1375–1383.

Shanmugam, B. K., H. Vardhan, M. G. Raj, M. Kaza, R. Sah, and H. Hanumanthappa. 2022. "Application of Fractional Factorial Design for Evaluating the Separation Performance of the Screening Machine." *International Journal of Coal Preparation and Utilization* 42, no. 11: 3369–3379.

Sharma, A., S. C. Sahoo, G. Kumar, S. K. Mehta, and R. Kataria. 2021. "Synthesis and Characterization of 1D-Co/Zn MOFs Having Potential for Efficient Dye Adsorption From Wastewater." *Journal of Molecular Structure* 1226: 129327–129335.

Silos-Llamas, A. K., G. Durán-Jiménez, V. Hernández-Montoya, M. A. Montes-Morán, and N. A. Rangel-Vázquez. 2020. "Understanding the Adsorption of Heavy Metals on Oxygen-Rich Biochars by Using Molecular Simulation." *Journal of Molecular Liquids* 298: 112069.

Thommes, M., K. Kaneko, A. V. Neimark, et al. 2015. "Physisorption of Gases With Special Reference to the Evaluation of Surface Area and Pore Size Distribution (IUPAC Technical Report)." *Pure and Applied Chemistry* 87: 1051–1069.

Tian, S., Y. Gong, H. Ji, J. Duan, and D. Zhao. 2020. "Efficient Removal and Long-Term Sequestration of Cadmium From Aqueous Solution Using Ferrous Sulfide Nanoparticles: Performance, Mechanisms, and Long-Term Stability." *Science of the Total Environment* 704: 135402.

Tran, H. N., S. J. You, and H. P. Chao. 2016. "Thermodynamic Parameters of Cadmium Adsorption Onto Orange Peel Calculated From Various Methods: A Comparison Study." *Journal of Environmental Chemical Engineering* 4, no. 3: 2671–2682.

Tran, H. N., S. J. You, A. Hosseini-Bandegharaei, and H. P. Chao. 2017. "Mistakes and Inconsistencies Regarding Adsorption of Contaminants From Aqueous Solutions: A Critical Review." *Water Research* 120: 88–116.

Varjani, S., G. Kumar, and E. R. Rene. 2019. "Developments in Biochar Application for Pesticide Remediation: Current Knowledge and Future Research Directions." *Journal of Environmental Management* 232: 505–513.

Wan, D., L. Wu, Y. Liu, H. Zhao, J. Fu, and S. Xiao. 2018. "Adsorption of Low Concentration Perchlorate From Aqueous Solution Onto Modified Cow Dung Biochar: Effective Utilization of Cow Dung, an Agricultural Waste." *Science of the Total Environment* 636: 1396–1407.

Wen, Y., P. Zhang, V. K. Sharma, X. Ma, and H. C. Zhou. 2021. "Metal-Organic Frameworks for Environmental Applications." *Cell Reports Physical Science* 2, no. 2: 100348.

Xu, C., R. Fang, R. Luque, L. Chen, and Y. Li. 2019. "Functional Metal–Organic Frameworks for Catalytic Applications." *Coordination Chemistry Reviews* 388: 268–292.

Xu, W., Y. Song, K. Dai, S. Sun, G. Liu, and J. Yao. 2018. "Novel Ternary Nanohybrids of Tetraethylenepentamine and Graphene Oxide Decorated With $MnFe_2O_4$ Magnetic Nanoparticles for the Adsorption of Pb (II)." *Journal of Hazardous Materials* 358: 337–345.

Yaashikaa, P. R., S. P. Kumar, S. Varjani, and A. Saravanan. 2020. "A Critical Review on the Biochar Production Techniques, Characterization, Stability and Applications for Circular Bioeconomy." *Biotechnology Reports* 28: e00570.

Yang, C., T. Ju, X. Wang, et al. 2020. "The Preparation of a Novel iron/Manganese Binary Oxide for the Efficient Removal of Hexavalent Chromium [Cr (VI)] from Aqueous Solutions." *RSC Advances* 10: 10612–10623.

Yang, Z., X. Chen, S. Li, et al. 2020. "Effective Removal of Cd (II) From Aqueous Solution Based on Multifunctional Nanoporous Silicon Derived From Solar Kerf Loss Waste." *Journal of Hazardous Materials* 385: 121522.

Yurdakal, S., C. Garlisi, L. Özcan, M. Bellardita, and G. Palmisano. 2019. "Chapter 4—(Photo)Catalyst Characterization Techniques: Adsorption Isotherms and BET, SEM, FTIR, UV-Vis, Photoluminescence and Electrochemical Characterizations." In *Heterogeneous Photocatalysis*, edited by G. Marcì and L. Palmisano, 87–152. Elsevier.

Zamora-Ledezma, C., D. Negrete-Bolagay, F. Figueroa, et al. 2021. "Heavy Metal Water Pollution: A Fresh Look About Hazards, Novel and Conventional Remediation Methods." *Environmental Technology & Innovation* 22: 101504.

Zhang, W., W. Du, F. Wang, et al. 2020. "Comparative Study on Pb^{2+} Removal From Aqueous Solutions Using Biochars Derived From cow Manure and Its Vermicompost." *Science of the Total Environment* 716: 137108.

Zhao, M. W. S., Y. Li, H. Wang, P. Qin, and F. Kong. 2019b. "Competitive Adsorption of Cu^{2+}, Pb^{2+}, Zn^{2+} and Cd^{2+} by New-Sodium Titanate Filler." *Acta Scientiae Circumstantiae* 39: 390–398.

Zhao, Y. L. D., Y. Dai, Y. Chen, G. Fu, and Y. Xu. 2019a. "Characteristics of Lead and Cadmium Adsorption by Drinking Water Treatment Residuals." *Research in Environmental Science* 32: 1250–1258.